Journal of Earth Science, *Vol. 29*, *No. 2*, *p. 326–341*, *April 2018* *ISSN 1674-487X*
Printed in China
https://doi.org/10.1007/s12583-017-0759-z

A Transgressive Depositional Setting for the Paleogene Shahejie Formation in the Qikou Depression, Eastern China: Inferences from the REE Geochemistry of Carbonates

Yang Yang[1], **Fuhong Gao**[*2], **Changwei Chen**[3], **Xiugang Pu**[3]
1. *School of Prospecting & Surveying Engineering*, *Changchun Institute of Technology*, *Changchun* 130061, *China*
2. *College of Earth Sciences*, *Jilin University*, *Changchun* 130061, *China*
3. *Research Institute of Exploration and Development*, *Dagang Oilfield Company*, *CNPC*, *Tianjin* 300280, *China*
Yang Yang: https://orcid.org/0000-0002-7494-7294; Fuhong Gao: https://orcid.org/0000-0001-6722-623X

ABSTRACT: Rare earth element (REE) and Y concentrations, and $^{87}Sr/^{86}Sr$ ratios were analyzed in 33 carbonate samples from the Paleogene Shahejie Formation in the Qikou depression, eastern China, with the goal of determining depositional environments and post-depositional conditions of carbonates in the region. The REE and Y concentrations were normalized to the post-Archean Australian shale (PAAS) standard. The La^*_{PAAS}/Yb^*_{PAAS} ratios of 0.35–1.52, where $*_{PAAS}$ indicates values for the PAAS standard, show light REE enrichment and heavy REE depletion in most samples. Values of La^*_{PAAS} (0.775–1.284) and Ce^*_{PAAS} (0.822–1.224), coupled with a relatively flat REE distribution, indicate that the Shahejie carbonates were deposited in lacustrine environments. Values of Y anomalies (1.009–1.527) and Y/Ho ratios (28.43–45.00) in the Shahejie Formation are greater than those of lacustrine carbonates and closer to those of marine carbonates, indicating that diagenetic fluids were probably influenced by seawater. In the carbonates from Well Kou-42, Eu anomalies (1.171–1.604), $^{87}Sr/^{86}Sr$ ratios (0.708 001–0.710 893), and high homogenization temperatures (104–151 ºC) suggest that the carbonates were affected by hydrothermal fluids. The REEs and Sr isotope ratios show that the carbonates from the Shahejie Formation in the Qikou depression were deposited in lacustrine environments, and were influenced by seawater and hydrothermal fluids.

KEY WORDS: Paleogene, carbonate, REE, Qikou depression.

0 INTRODUCTION

Carbonate rock formations are important reservoirs of oil and gas, and the origins of diagenetic fluids and depositional environments of carbonates are topics of active research (Li et al., 2014; Yang et al., 2013; Zheng et al., 2013; Ge et al., 2010; Bolhar and Van Kranendonk, 2007; Drummond et al., 1995; Curtis et al., 1986). Carbonates are precipitated from oceanic, continental, and marginal-basin waters, and when precipitated at thermodynamic equilibrium, they can serve as proxies for the geochemical records of elements and isotopes in the basin waters from which they originate. Rare earth element (REE) concentrations in chemical sediments have provided useful information on depositional environments of carbonates and the fluids from which these rocks originate (Frimmel, 2009; Wright et al., 1987). It is well known that geochemical signatures of REEs are powerful indicators of chemical processes occurring in carbonate depositional environments (Haley et al., 2004), as the distribution of REEs is sensitive to water depth, salinity, and oxygen levels (Frimmel, 2009).

The distributions of REEs in carbonates are the result of interactions between diagenetic fluids and the carbonate substrate (Han et al., 2009). The REE patterns and anomalies with respect to Ce, Eu, and Y have been used to distinguish between oceanic, continental, and hydrothermal sediments. Reliably preserved REE signatures in ancient sedimentary provide clues to the evolution of paleoenvironmental conditions (Frimmel, 2009; Bolhar and Van Kranendonk, 2007; Li et al., 2007; Brenchley et al., 2003). While strontium isotope stratigraphy has been predominantly used for correlation and dating of marine sediments (McArthur, 1994; Veizer et al., 1989; Elderfield, 1986), strontium isotope signatures can also be used to distinguish between marine and freshwater environments (Schmitz et al., 1991) and to identify reworking in sediments (MacLeod and Huber, 1996).

The possibility of a Paleogene transgression in the Bohaiwan Basin, which has been discussed for more than 20 years, is still an unresolved issue. Evidence for transgression includes markers such as glauconite, apatite, sponge, calcareous nannofossils, ostracods, gastropods, marine trace fossils, and particular stable isotope, trace element, and organic signatures (Wu

*Corresponding author: gaofh@jlu.edu.cn

Manuscript received March 5, 2016.
Manuscript accepted December 14, 2016.

and Ren, 2004; Ren et al., 2000; Li et al., 1997; Yao et al., 1992; Li and Xiao, 1988; Zhao and Liu, 1988; Zhang and Wang, 1987; Chen et al., 1982; Yu, 1982). However, the geochemical evidence, which only reflects water salinities under certain conditions, is not useful for distinguishing between marine and freshwater environments (Yao et al., 1992). Moreover, no marine connection has been discovered (Tong, 1985), and the minerals and fossils in the Bohaiwan Basin show characteristics of circular distribution, which is indicative of a lake environment rather than a marine environment (Sun et al., 1997). The question remains as to whether the Shahejie carbonates present atypical characteristics of marine deposition. In this study, REE characteristics, strontium isotopes, and associated petrological characteristics of carbonates from two wells in the Shahejie carbonates in the Qikou depression were analyzed to investigate the possibility of a Paleogene transgression and to quantify the post-depositional processes affecting the carbonates.

1 GEOLOGICAL SETTING AND STRATIGRAPHIC BACKGROUND

The Huanghua depression, located in the central area of the Bohaiwan Basin, China, is a pull-apart structure within the North China Craton. The Huanghua depression is bounded by the Cangdong uplift in the west and the Bozhong depression in the east; the depression, which presently extends in an ENE-WSW direction, represents a region of extensive crustal stretching in the Bohaiwan area. The largest negative structural unit in the Huanghua depression is the Qikou depression. The Qikou depression, with a total area of 3 800 km^2 and a terrestrial area of 1 100 km^2, is located in the central northern area of the Huanghua depression, and is the largest hydrocarbon source area in the Huanghua depression (Fig. 1). Within the context of the geological history of the Huanghua depression, the sedimentary evolution of the Qikou depression can be divided into four stages: (1) initial fault-controlled depression, (2) rapid rifting, (3) stable rifting, and (4) fault-controlled downwarping.

Most basement faults in the Qikou depression are normal faults that formed after the Indo-Chinese Epoch (257–205 Ma). According to structural associations, the basement faults can be classified into primary and secondary faults. Primary faults include the Yangerzhuang Fault and the Cangdong Fault, which played important roles in the development of the Huanghua depression and controlled the spatiotemporal distributions of sedimentary units. Secondary faults, which comprise the Gangdong, Nandagang, Yangbei, Koucun and Zhaobei faults, controlled the formation of oil and gas reservoirs (Fig. 1).

The Paleogene sedimentary sequence in the Qikou depression is of the order of 10^4 m thick, and comprises, from the base upwards, the Kongdian Formation, Shahejie Formation, and

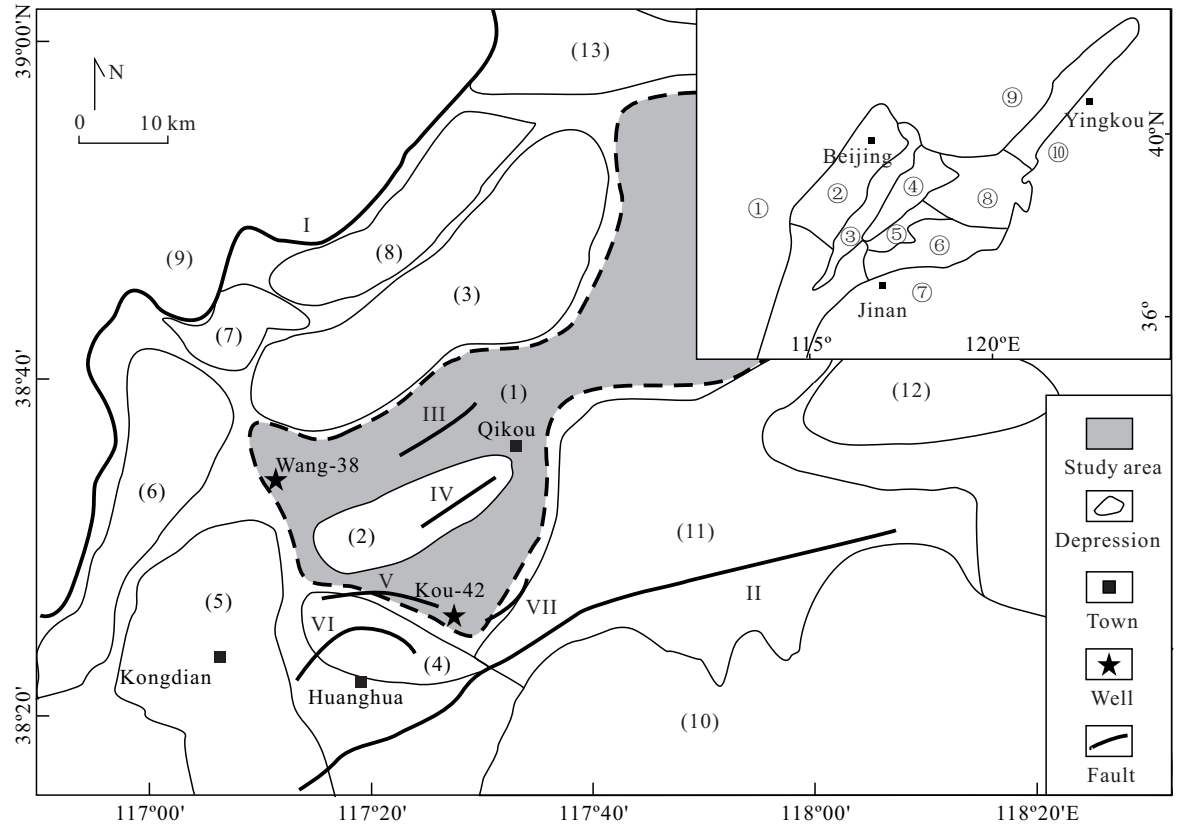

Figure 1. Well location in the Qikou depression, modified after Pu et al. (2011). (1) Qikou depression, (2) Nandagang buried hill, (3) Beidagang buried hill, (4) Yangsanmu uplift, (5) Kongdian uplift, (6) Cangdong depression, (7) Shenqingzhuang buried hill, (8) Banqiao depression, (9) Cangxian uplift, (10) Chengning uplift, (11) Chengbei fault step, (12) Shanan depression, (13) Tangguxingang buried hill; ①Taihangshan uplift, ② Jizhong depression, ③ Cangxian uplift, ④ Huanghua depression, ⑤ Chengning uplift, ⑥ Jiyang depression, ⑦ Luxi uplift, ⑧ Bozhong depression, ⑨ Shanhaiguan uplift, ⑩ Jiaoliao uplift; I. Cangdong fault, II. Yangerzhuang fault, III. Gangdong fault, IV. Nandagang fault, V. Yangbei fault, VI. Koucun fault, VII. Zhaobei fault.

Dongying Formation. The Shahejie Formation is further divided (from the base upwards) into Shahejie III (Es_3), Shahejie II (Es_2), and Shahejie I (Es_1). The Es_3 is composed of conglomerate, sandstone, pelitic siltstone, mudstone, and oil shale. The Es_2 is composed mainly of argillaceous, pebbly sandstone, mudstone, and dolostone. The Es_1 consists of mudstone, shale, bioclastic limestone, and dolostone (Li et al., 1991).

2 SAMPLES AND ANALYTICAL METHODS

Thirty-three samples were collected from wells Kou-42 and Wang-38 (Fig. 2). Calcite spar was removed from the samples under a microscope using a dental drill. The carbonate surface was lightly etched with dilute 10% HCl to enable calcite to be distinguished from dolomite. Several grams of samples were pulverized to less than 200 mesh sizes for analysis. The present measurement is focused on the Es_1–Es_2 transition that spans the Eocene and Oligocene, results are shown in Tables 1 and 2.

Major element and REE compositions were determined using an ME-MS82 inductively coupled plasma-mass spectrometer (ICP-MS) housed at the Australian Laboratory Services (ALS) Laboratory, Guangzhou, China (an ISO/IEC 17025: 2005 accredited facility). Analytical results obtained for

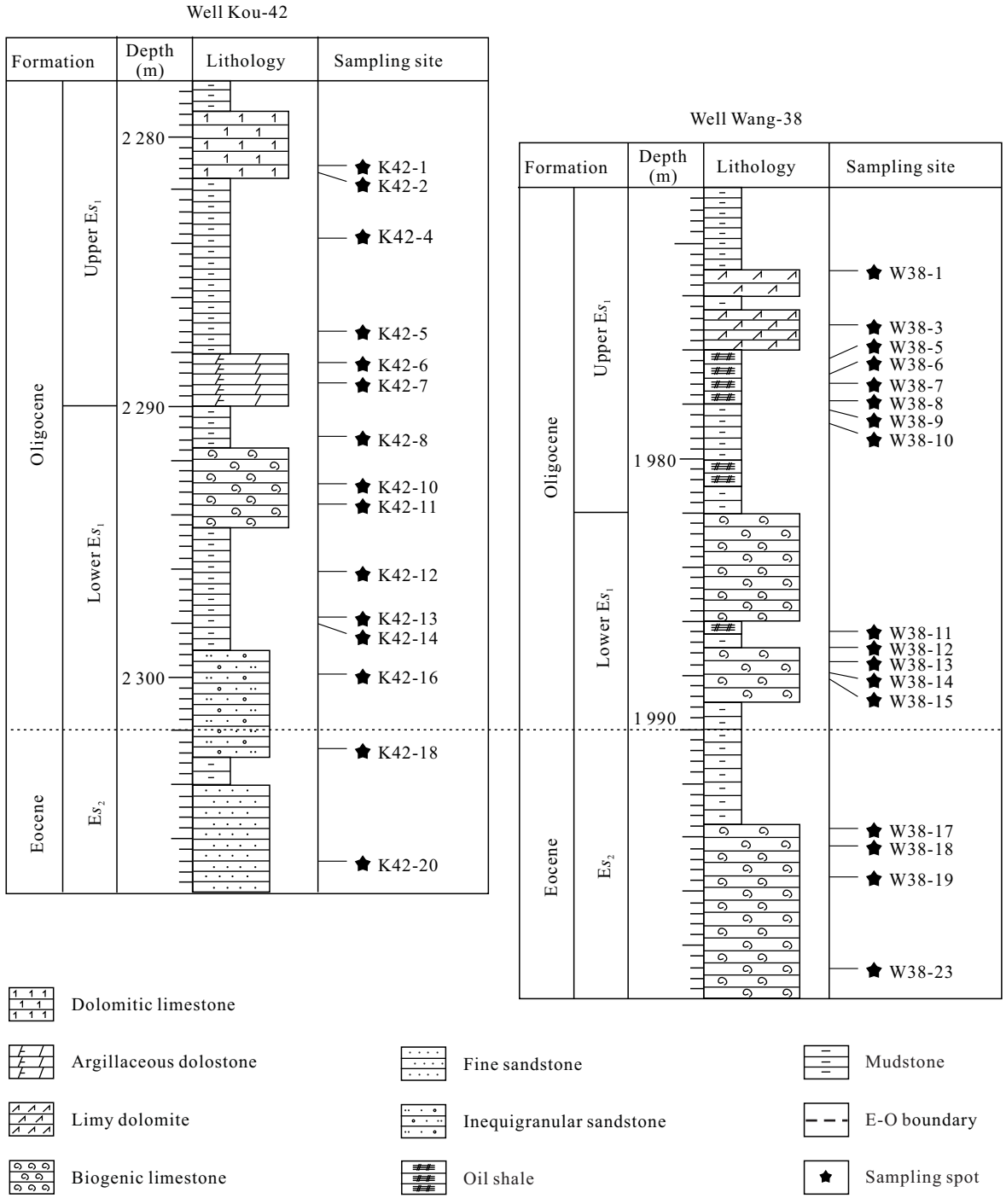

Figure 2. Stratigraphic sequences and locations of samples in wells Kou-42 and Wang-38.

Table 1 Continued

Sample No.	Depth (m)	Lithology	Formation	La	Ce	Pr	Nd	Sm	Eu	Gd	Tb	Dy	Y	Ho	Er	Tm	Yb	Lu
w38-14	1 987.90	Bioclast limestone limestone	Lower	1.100	2.700	0.340	1.400	0.310	0.110	0.330	0.040	0.330	2.700	0.060	0.220	0.030	0.230	0.020
w38-15	1 988.09	Bioclast limestone limestone	Es_1	9.000	19.100	2.400	8.700	1.520	0.350	1.380	0.190	1.180	7.200	0.220	0.710	0.100	0.720	0.080
Average				6.200	13.260	1.656	6.260	1.212	0.338	1.156	0.166	1.046	6.980	0.202	0.636	0.086	0.604	0.074
w38-17	1 993.68	Limestone		18.200	37.700	4.790	17.800	3.430	0.840	3.280	0.490	2.850	16.800	0.590	1.720	0.240	1.620	0.220
w38-18	1 994.30	Bioclast limestone	Es_2	16.000	33.700	4.270	16.200	3.270	0.780	3.140	0.480	2.800	17.000	0.560	1.620	0.230	1.510	0.200
w38-19	1 995.51	Bioclast limestone		15.100	32.300	4.210	15.600	3.190	0.740	2.990	0.460	2.710	16.200	0.550	1.590	0.230	1.510	0.210
w38-23	1 998.85	Dolomicrite		19.300	39.600	5.070	18.500	3.440	0.730	2.970	0.460	2.580	14.500	0.510	1.480	0.210	1.370	0.200
Average				17.150	35.825	4.585	17.025	3.333	0.773	3.095	0.473	2.735	16.125	0.553	1.603	0.228	1.503	0.208
Green River Formation				0.318	0.780	0.088	0.343	0.071	0.017	0.069	0.011	0.068	0.430	0.015	0.042		0.042	0.006

GSR-12 (dolostone) and GSR-13 (limestone) standards indicate that the precision for REE determinations was better than 5%.

Strontium separation was performed using a 50-μL column and Sr-specific resin (Eichrom Technologies). Isotopic analysis of a solution containing 300 ng Sr was performed using a Nu multi-collector-inductively coupled plasma-mass spectrometer (MC-ICP-MS) housed at the State Key Laboratory of Geological Processes and Mineral Resources, China University of Geosciences, Wuhan, China. Reagents and column blanks contained <10 ng Sr. The $^{87}Sr/^{86}Sr$ data were normalized to the NBS-987 standard ($^{87}Sr/^{86}Sr$=0.710 24); we obtained a mean $^{87}Sr/^{86}Sr$ value of 0.710 20±0.000 05 (mean ±2σ; n=50) for repeated measurements of the standard.

Determinations of the temperatures of homogenous of fluid inclusions were performed at the Geologic Experiment Center, College of Earth Sciences, Jilin University, Changchun, China. Thirteen double-polished 1-cm^2 carbonate wafers were selected for microthermometric determinations, which were performed on a Linkam THMS-600 heating-freezing stage calibrated to the triple point of distilled water (0.0 °C) and pure CO_2-bearing fluid inclusions (-56.6 °C). The accuracy of the measurements was approximately ±0.2 °C for both freezing and heating runs, results are showed in Table 3.

3 ANALYTICAL RESULTS

The REE and Y data for all carbonates are presented in shale-normalized diagrams (Figs. 3a, 3b), using the post-Archean Australian shale (PAAS) standard (Taylor and McLennan, 1985) for normalization. Equations used to calculate elemental anomalies are: $La/La^*_{PAAS}=La_{PAAS}/(3Pr_{PAAS}-2Nd_{PAAS})$, $Ce/Ce^*_{PAAS}=Ce_{PAAS}/(2Pr_{PAAS}-Nd_{PAAS})$, $Eu/Eu^*_{PAAS}=Eu_{PAAS}/(0.67Sm_{PAAS}+0.33Tb_{PAAS})$, $Gd/Gd^*_{PAAS}=Gd_{PAAS}(2Tb_{PAAS}-Dy_{PAAS})$, and $Y/Y^*_{PAAS}=2Y_{PAAS}(Dy_{PAAS}+Ho_{PAAS})$, where $^*_{PAAS}$ represents values for the PAAS standard.

3.1 Well Kou-42

Carbonates of Es_2 have low initial $^{87}Sr/^{86}Sr$ ratios of 0.708 979–0.709 191; they show flat REE+Y patterns, $(La/Yb)_{PAAS}$ ratios of 0.94–1.23, and are characterized by: (1) minor negative Ce anomalies, with Ce/Ce^*_{PAAS} ratios of 0.983–0.997; (2) positive Eu and Y anomalies, with Eu/Eu^*_{PAAS} ratios of 1.195–1.206 and Y/Y^*_{PAAS} ratios of 1.089–1.107; (3) variable Gd anomalies, with Gd/Gd^*_{PAAS} ratios of 0.973–1.101; and (4) Y/Ho ratios of 29.38–30.00 (Tables 1, 2).

Carbonates of the lower Es_1 have low initial $^{87}Sr/^{86}Sr$ ratios of 0.708 001–0.710 359. Most samples are enriched in light REEs (LREEs) relative to heavy REEs (HREEs), with La/Yb_{PAAS} ratios of 1.02–1.67. The REE+Y patterns of lower Es_1 carbonates are characterized by: (1) variable Ce and Gd anomalies, with Ce/Ce^*_{PAAS} ratios of 0.983–1.224 and Gd/Gd^*_{PAAS} ratios of 0.907–1.091; (2) positive La, Eu, and Y anomalies, with La/La^*_{PAAS} ratios of 1.021–1.284, Eu/Eu^*_{PAAS} ratios of 1.228 2–1.604, and Y/Y^*_{PAAS} ratios of 1.088–1.239; and (3) Y/Ho ratios of 31.00–34.17 (Tables 1, 2).

Residues have high initial $^{87}Sr/^{86}Sr$ ratios of 0.710 072–0.710 893. The REE+Y patterns are flat, with $(La/Yb)_{PAAS}$ ratios of 0.87–1.41. The residues are characterized by: (1) variable Gd anomalies, with Gd/Gd^*_{PAAS} ratios of 0.901–1.064; (2) positive

Table 2 The geochemical features of carbonates from the Shahejie Formation, Qikou depression

Sample No.	Depth (m)	Lithology	Formation	REE (ppm)	La/La*	Ce/Ce*	Gd/Gd*	Eu/Eu*	Y/Y*	La/Yb	Dy/Sm	La/Sm	Y/Ho	$^{87}Sr/^{86}Sr$	$\pm 2\sigma$
k42-1	2 281.09	Dolomicrite		32.77	1.136	1.156	1.064	1.445	1.237	0.97	1.02	0.95	33	0.708 053	5
k42-2	2 281.40	Dolomicrite		63.41	1.201	1.178	0.955	1.313	1.120	0.87	1.21	1.10	30	0.710 893	4
k42-4	2 285.74	Argillaceous dolostone	Upper	121.08	1.172	1.054	0.963	1.171	1.068	1.41	0.89	1.04	30	0.710 283	4
k42-5	2 287.25	Dolomicrite	Es_1	141.16	1.163	1.057	0.954	1.177	1.077	1.12	0.94	0.96	30	0.710 095	4
k42-6	2 288.24	Dolomicrite		39.03	1.179	1.157	0.934	1.371	1.095	1.22	0.92	0.97	31	0.710 072	5
k42-7	2 289.15	Dolomicrite		39.96	1.286	1.227	0.901	1.330	1.081	1.25	0.93	1.02	30	0.710 496	4
Average					1.206	1.224	0.927	1.269	1.089	1.04	0.98	0.94	30	0.710 359	
k42-8	2 291.07	Dolomicrite		72.28	1.206	1.224	0.927	1.269	1.089	1.04	0.98	0.94	30	0.710 359	4
k42-10	2 292.88	Dolomicrite		77.87	1.284	1.204	0.907	1.274	1.163	0.83	1.09	0.96	31	0.709 773	4
k42-11	2 293.62	Dolomicrite		22.94	1.261	1.135	1.069	1.471	1.241	1.15	1.00	1.05	34	0.710 195	3
k42-12	2 296.07	Argillaceous dolostone	Lower	110.52	1.060	1.131	1.003	1.228	1.150	1.09	0.91	0.92	31	0.710 07	5
k42-13	2 297.79	Bioclast limestone	Es_1	27.22	1.110	1.028	0.970	1.524	1.147	1.02	1.00	0.82	32	0.709 507	4
k42-14	2 298.02	Bioclast limestone limestone		54.09	1.021	0.988	1.029	1.480	1.106	1.38	0.79	0.92	31	0.709 429	4
k42-15	2 299.88	Bioclast limestone limestone		71.14	1.081	0.983	1.031	1.279	1.171	1.29	0.83	1.23	31	0.709 046	4
k42-16	2 301.50	Bioclast limestone limestone		29.67	1.165	1.053	1.091	1.604	1.095	1.67	0.68	1.11	31	0.708 001	5
Average					1.149	1.093	1.003	1.391	1.145	1.18	0.91	0.99	32	0.709 548	
k42-18	2 302.64	Bioclast limestone limestone		102.90	1.069	0.997	1.001	1.206	1.090	1.23	0.81	1.03	29	0.708 979	5
k42-20	2 306.79	Bioclast limestone limestone	Es_2	56.24	0.998	0.983	0.973	1.195	1.107	0.94	1.07	1.02	30	0.709 191	4
Average					1.034	0.990	0.987	1.200	1.099	1.09	0.94	1.03	30	0.709 085	
w38-1	1 972.99	Argillaceous dolostone		207.34	1.052	1.041	1.100	1.094	1.072	1.52	0.75	1.02	30	0.710 383	5
w38-3	1 974.94	Dolomicrite		128.04	1.032	1.150	1.036	1.145	1.075	1.18	0.91	1.04	30	0.710 724	5
w38-5	1 976.30	Dolomicrite		66.70	1.044	1.118	1.065	1.173	1.176	0.81	1.12	0.86	32	0.710 377	6
w38-6	1 976.60	Dolomicrite	Upper	69.41	1.187	1.203	0.986	1.247	1.188	0.87	1.07	0.91	32	0.710 337	7
w38-7	1 977.19	Argillaceous dolostone	Es_1	154.70	1.119	1.076	1.080	1.119	1.095	1.37	0.85	1.00	31	0.710 638	5
w38-8	1 977.90	Dolomicrite		142.90	1.100	1.066	1.073	1.147	1.125	1.48	0.87	1.10	31	0.710 265	4
w38-9	1 978.21	Dolomicrite		180.82	1.049	1.012	1.080	1.111	1.027	1.47	0.82	1.14	29	0.710 415	3
w38-10	1 978.70	Dolomicrite		125.69	0.792	0.775	1.082	1.135	1.010	1.26	0.82	0.81	29	0.710 523	6
Average					1.047	1.055	1.063	1.146	1.096	1.25	0.90	0.98	30	0.710 458	
w38-11	1 986.45	Bioclast limestone limestone	Lower	19.51	0.856	0.859	1.234	2.592	1.338	0.53	1.25	0.67	38	0.710 282	5
w38-12	1 986.95	Bioclast limestone limestone	Es_1	59.60	0.876	0.916	1.091	1.203	1.174	0.82	1.00	0.72	33	0.710 348	4

Table 2 Continued

Sample No.	Depth (m)	Lithology	Formation	REE (ppm)	La/La*	Ce/Ce*	Gd/Gd*	Eu/Eu*	Y/Y*	La/Yb	Dy/Sm	La/Sm	Y/Ho	$^{87}Sr/^{86}Sr$	$\pm 2\sigma$
w38-13	1 987.50	Bioclast limestone limestone	Lower Es_1	32.50	0.855	0.855	1.240	1.289	1.176	0.80	0.99	0.74	34	0.710 585	3
w38-14	1 987.90	Bioclast limestone limestone		7.22	0.875	0.950	2.156	1.870	1.527	0.35	1.26	0.52	45	0.710 5	4
w38-15	1 988.09	Bioclast limestone limestone		45.65	0.780	0.836	1.240	1.225	1.126	0.92	0.92	0.86	33	0.710 498	6
Average					0.848	0.883	1.392	1.636	1.268	0.68	1.08	0.70	36	0.710 443	
w38-17	1 993.68	Limestone	Es_2	93.77	0.825	0.846	1.071	1.248	1.034	0.83	0.99	0.77	28	0.710 348	4
w38-18	1 994.30	Bioclast limestone		84.76	0.846	0.865	1.050	1.205	1.083	0.78	1.02	0.71	30	0.710 259	4
w38-19	1 995.51	Bioclast limestone		81.39	0.775	0.822	1.053	1.179	1.059	0.74	1.01	0.69	29	0.710 285	5
w38-23	1 998.85	Dolomicrite		96.42	0.801	0.826	1.000	1.106	1.009	1.04	0.89	0.82	28	0.710 542	4
Average				89.085	0.812	0.840	1.043	1.184	1.046	0.85	0.97	0.75	29	0.710 359	
Green River Formation					0.862	0.998	1.066	1.187	1.075				29		

La/Yb, Dy/Sm, La/Sm, La/La*, Ce/Ce*, Gd/Gd*, Eu/Eu* and Y/Y* ratios are calculated by the PAAS-normalization.

La, Ce, Eu, and Y anomalies, with La/La*$_{PAAS}$ ratios of 1.136–1.286, Ce/Ce*$_{PAAS}$ ratios of 1.054–1.227, Eu/Eu*$_{PAAS}$ ratios of 1.171–1.445, and Y/Y*$_{PAAS}$ ratios of 1.067–1.236; and (3) Y/Ho ratios of 29.50–33.16 (Tables 1, 2).

3.2 Well Wang-38

Carbonates of Es_2 have high initial $^{87}Sr/^{86}Sr$ ratios of 0.710 259–0.710 542, consistently flat REE+Y patterns, and (La/Yb)$_{PAAS}$ ratios of 0.78–1.04. The Es_2 carbonates are characterized by: (1) negative La and Ce anomalies, with La/La*$_{PAAS}$ ratios of 0.775–0.846 and Ce/Ce*$_{PAAS}$ ratios of 0.822–0.865; (2) positive Gd, Eu, and Y anomalies, with Gd/Gd*$_{PAAS}$ ratios of 1.000–1.071, Eu/Eu*$_{PAAS}$ ratios of 1.106–1.248, and Y/Y*$_{PAAS}$ ratios of 1.148–1.233; and (3) Y/Ho ratios of 28.43–30.36 (Tables 1, 2).

Carbonates of lower Es_1 have high initial $^{87}Sr/^{86}Sr$ ratios of 0.710 348–0.710 585 and are enriched in HREEs, with La/Yb$_{PAAS}$ ratios of 0.35–0.92. The lower Es_1 carbonates are characterized by: (1) negative La and Ce anomalies, with La/La*$_{PAAS}$ ratios of 0.780–0.876 and Ce/Ce*$_{PAAS}$ ratios of 0.836–0.950; (2) positive Gd, Eu, and Y anomalies, with Gd/Gd*$_{PAAS}$ ratios of 1.091–2.156, Eu/Eu*$_{PAAS}$ ratios of 1.203–2.592, and Y/Y*$_{PAAS}$ ratios of 1.285–1.745; and (3) Y/Ho ratios of 32.73–34.21 (Tables 1, 2).

Residues have high initial $^{87}Sr/^{86}Sr$ ratios of 0.710 383–0.710 727 and show flat REE+Y patterns, with (La/Yb)$_{PAAS}$ ratios of 0.81–1.52. They are characterized by: (1) variable La, Ce, and Gd anomalies, with La/La*$_{PAAS}$ ratios of 0.792–1.187, Ce/Ce*$_{PAAS}$ ratios of 0.775–1.203, and Gd/Gd*$_{PAAS}$ ratios of 0.986–1.082; (2) positive Eu and Y anomalies, with Eu/Eu*$_{PAAS}$ ratios of 1.094–1.247 and Y/Y*$_{PAAS}$ ratios of 1.009–1.187; and (3) Y/Ho ratios of 28.71–30.55 (Tables 1, 2).

4 DISCUSSION

4.1 Non-Carbonate Contamination and Primitive REE Compositions

Carbonate REE+Y concentrations can be influenced by contamination of non-carbonate materials, such as silicates, Fe-Mn oxides, phosphates, and sulfides during chemical leaching. Thus, the REE+Y concentrations of sedimentary carbonates can only be reliably used to infer ancient water chemistry and the characteristics of depositional environments if complications related to contamination can be ruled out. In our study, we took several approaches to minimize non-carbonate contamination, including: (1) collection of individual samples at fresh outcrops to avoid contamination by materials associated with shale beds; (2) use of samples that consist mainly of microcrystalline calcite and dolomite, and which show no evidence of recrystallization or metamorphism when viewed under the microscope; and (3) after crushing, careful handpicking of only the material that was free of non-carbonates.

During their formation, carbonates incorporate Sr isotope compositions (Stille et al., 1996, 1994; Stille, 1992; Grandjean et al., 1987; Shaw and Wasserburg, 1985) and REE patterns similar to those of the diagenetic fluids in which they precipitated (Sholkovitz and Shen, 1995; Grandjean et al., 1987; Wright et al., 1987; Palmer and Elderfield, 1986). The REE patterns may be subsequently altered by post-depositional

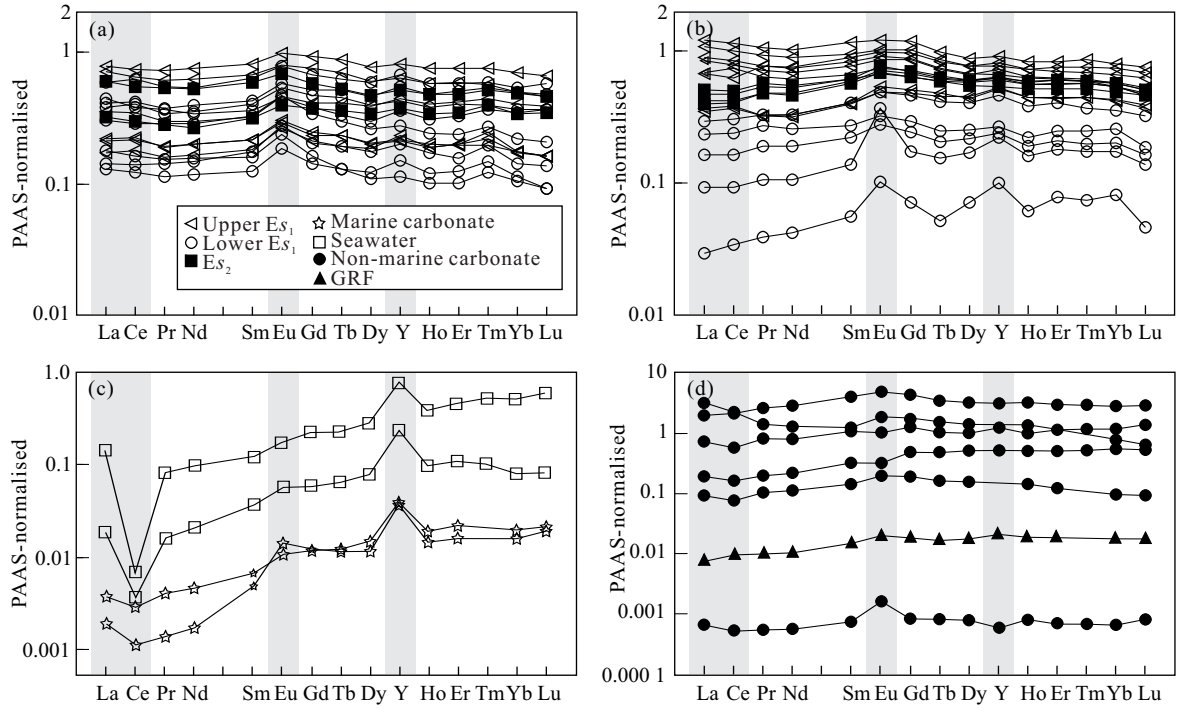

Figure 3. Plots of PAAS-normalized REE and Y concentrations of carbonates from the Shahejie Formation, Qikou depression. Data sources: Bolhar and Van Kranendonk (2007); Alibo and Nozaki (2004); Van Kranendonk et al. (2003); Webb and Kamber (2000); Zhang and Nozaki (1996).

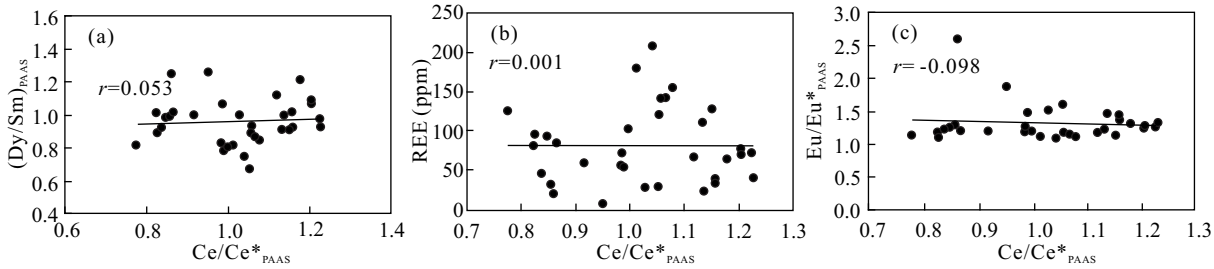

Figure 4. Correlations between Ce/Ce^*_{PAAS} ratios and Dy_{PAAS}/Sm_{PAAS} ratios (a), Ce/Ce^*_{PAAS} and Eu/Eu^*_{PAAS} (b), and Ce/Ce^*_{PAAS} and w(REE) (c) of carbonates from the Shahejie Formation, Qikou depression.

Table 3 Homogenization temperatures of fluid inclusions from carbonates in wells Kou-42 and Wang-38

Sample No.	Depth (m)	Lithology	Formation	Homogenization temperatures (ºC)
k42-13	2 297.79	Bioclast limestone	Lower Es_1	104, 108, 118, 124
k42-14	2 298.02	Bioclast limestone	Lower Es_1	119, 124, 131, 137, 138
k42-15	2 299.88	Bioclast limestone	Lower Es_1	119, 123, 125, 125, 128
k42-16	2 301.50	Bioclast limestone	Lower Es_1	136, 140, 142, 145, 146, 148, 151
k42-17	2 306.79	Bioclast limestone	Lower Es_1	132, 138, 138, 145, 146
k42-18	2 302.64	Bioclast limestone	Es_2	124, 127, 131, 136, 138
w38-12	1 986.95	Bioclast limestone	Lower Es_1	83, 85, 94, 95, 100
w38-13	1 987.50	Bioclast limestone	Lower Es_1	98, 109, 118, 113, 123
w38-14	1 987.90	Bioclast limestone	Lower Es_1	94, 96, 101, 101, 103
w38-16	1 993.19	Bioclast limestone	Es_2	99, 101, 101, 109, 112
w38-17	1 993.68	Limestone	Es_2	96, 98, 106, 118, 125
w38-19	1 995.51	Bioclast limestone	Es_2	90, 96, 98, 101
w38-22	1 997.93	Bioclast dolostone	Es_2	86, 89, 93, 101

diagenetic exchange (German and Elderfield, 1990) and surface weathering processes (Bonnot-Courtois and Flicoteaux, 1989; McArthur and Walsh, 1984). However, the concentrations of REEs in most geological fluids are low, reaching levels of 0.01 ppm only in hydrothermal fluids (McLennan, 1989). Therefore, the characteristics of the REE compositions in the original rock are generally well preserved.

A study by Shields and Stille (2001) showed a strong negative correlation between the $(Dy/Sm)_{PAAS}$ and Ce/Ce^*_{PAAS} ratios of basal Cambrian phosphorites in South China, which implies that Ce values have been significantly affected by medium REE (MREE) enrichment. The positive correlation between Ce/Ce^*_{PAAS} ratios and REE concentrations indicates that this Ce alteration was the result of progressive post-depositional REE scavenging. The strong negative correlation between Ce/Ce^*_{PAAS} and Eu/Eu^*_{PAAS} ratios further confirms that diagenetic processes have altered the Ce/Ce^*_{PAAS} ratios of most samples. In the present study, we observed no correlation between Ce/Ce^*_{PAAS} and $(Dy/Sm)_{PAAS}$, Ce/Ce^*_{PAAS} and Eu/Eu^*_{PAAS}, or Ce/Ce^*_{PAAS} and REE (Fig. 4), which indicates that the carbonates in the study area were not altered during diagenesis.

4.2 Implications For Sedimentary Environment

Small but systematic differences in the chemical properties of REE+Y components provide important insights into processes and sources of REEs in the hydrosphere and lithosphere (Hofmann and Bolhar, 2007; Bolhar et al., 2004, 2002; Shields and Webb, 2004; Van Kranendonk et al., 2003; Webb and Kamber, 2000; Bau and Möller, 1993). In contrast to REE+Y patterns in the vast majority of geological samples, the dissolved REEs+Y in oceanic, estuarine, and river waters do not display smooth abundance patterns as a function of ionic radius when normalized to PAAS; instead, significant abundance peaks are usually present for elements such as La, Ce, Eu, and Gd (Bolhar et al., 2004; Kamber et al., 2004; Van Kranendonk et al., 2003; Kamber and Webb, 2001; Webb and Kamber, 2000). Water La, Ce, Eu, Gd, and Y anomalies, as well as REE+Y patterns, reflect various complexation phenomena that are unique to the hydrosphere (Bolhar and Van Kranendonk, 2007). Hence, reliable uncontaminated intact proxies for different water chemistries can be recognized on the basis of REE+Y characteristics.

4.2.1 Lacustrine depositional environment

The REE distributions in seawater and marine carbonates are primarily controlled by the balance between marine hydrothermal and terrestrial weathering inputs, as modified by scavenging in estuarine and deep marine environments (Elderfield, 1986). Generally, normal marine carbonates in oxygenated seawater are characterized by: (1) uniform LREE depletion, (2) positive La anomalies, (3) positive Gd anomalies, and (4) negative Ce anomalies (Bolhar et al., 2004; Shields and Webb, 2004; Van Kranendonk et al., 2003; Webb and Kamber, 2000) (Fig. 3c). The REE+Y compositions of a lacustrine stromatolite from the Phanerozoic Green River Formation are presented in Table 1 for comparison. The Green River Formation is conspicuous in having a virtually flat REE+Y pattern and no anomalous elemental concentrations (Fig. 3d). The difference between the REE distributions of marine and lacustrine carbonates can be used to distinguish depositional paleoenvironments.

Positive La anomalies in chemical sedimentary rocks, calculated from PAAS-normalized REE+Y abundances, can be considered as reliable indicators of water chemistry (Kamber et al., 2004; Shields and Webb, 2004; Kamber and Webb, 2001; Bau, 1996). The La anomaly of freshwater (the average La/La^*_{PAAS} ratio is 2.62, depending on pH) is small in comparison with that of seawater (Lawrence et al., 2006). Carbonates of the Shahejie Formation have variable La anomalies, with La/La^*_{PAAS} ratios of 0.775 to 1.286 (Table 2); these ratios are lower than the average value of 2.62 for marine carbonates (Shields and Webb, 2004; Van Kranendonk et al., 2003; Webb and Kamber, 2000), but are similar to those of Green River Formation carbonates that were deposited in lacustrine settings (Bolhar et al., 2004).

The anomalous abundance spike of Ce can be explained by the redox behavior of Ce. Cerium can undergo oxidation in water from soluble Ce^{3+} to highly insoluble Ce^{4+}, a process that sets Ce apart from other REEs. Thus, the concentration of Ce relative to that of neighboring REEs has been used to deduce redox conditions in the water column at the time of REE uptake. In particular, the extent of Ce depletion reflects the oxygenation state of seawater (Frimmel, 2009). For example, Ce/Ce^*_{PAAS} ratios in typical seawater vary in the range of 0.1–0.4 (Piepgras and Jacobsen, 1992). Negative Ce anomalies (0.14) have been recorded in a Jurassic reef limestone from the southeast Pacific (DSDP Site 598; Olivarez and Owen, 1991), and Ce/Ce^*_{PAAS} ratios of 0.45 and 0.752 have been recorded in Cretaceous limestones of northern Italy and in Holocene reefal microbialites of the southern Great Barrier Reef, respectively (Webb and Kamber, 2000; Bellanca et al., 1997). The Shahejie carbonates have variable Ce anomalies, with Ce/Ce^*_{PAAS} ratios of 0.822–1.227 (Table 2), indicating that these carbonates were deposited under somewhat reducing lacustrine conditions.

Because the abundances of Eu in the Shahejie carbonates are variable, Gd contents are expressed relative to Tb and Dy, rather than Eu (Table 2). Depending on the method of calculation, the Shahejie carbonates show variable Gd/Gd^*_{PAAS} ratios fluctuating around a value of 1 (Table 2). A positive Gd anomaly is considered a proxy for Archean marine seawater (Kamber et al., 2004). However, positive Gd anomalies are also prevalent in freshwater environments (Lawrence et al., 2006). Hence, the presence of subtle positive Gd anomalies may not allow differentiation between lacustrine and marine environments of deposition (Bolhar and Van Kranendonk, 2007).

4.2.2 Transgressive depositional conditions

The REE+Y patterns of the Shahejie carbonates are analogous to those of the Green River Formation, indicating a lacustrine origin for both sediments; however, there are some differences in the elemental anomalies in the two formations. The La and Ce anomalies in the Shahejie carbonates are variable, while in the Green River Formation, the La/La^*_{PAAS} ratios show a negative anomaly and the Ce/Ce^*_{PAAS} ratios show a minor negative anomaly. Despite the fact that the Y/Y^*_{PAAS} ratios of the Shahejie carbonates and the Green River Formation are both positive, most Y/Y^*_{PAAS} ratios of the Shahejie carbonates are

considerably higher than those of the Green River Formation, and are close to values for marine carbonates (Figs. 3c, 3d). In addition, some of the Shahejie carbonates display obvious LREE depletion (Fig. 3b), which is in accord the LREE compositions of seawater and marine carbonates (Fig. 3d). Thus, the Shahejie carbonates have the characteristics of lacustrine carbonates; however, they are affected by marine conditions.

The Y/Ho ratios of marine carbonates are higher than those of freshwater carbonates (Bolhar et al., 2004; Shields and Webb, 2004; Van Kranendonk et al., 2003; Webb and Kamber, 2000). In aqueous environments, elevated concentrations of Y relative to Ho reflect differences in the complexation behavior of these elements, which have identical charge and near-identical effective ionic radii (Nozaki et al., 2000; Bau and Dulski, 1999). The Y/Ho ratios of modern seawater are substantially higher than those of river and estuarine waters (Lawrence et al., 2006; Nozaki et al., 2000, 1997). The Y/Ho ratios of carbonates in Archean and post-Archean microbialites deposited in marine settings are generally >40 (Bolhar and Van Kranendonk, 2007; Kamber et al., 2004; Van Kranendonk et al., 2003; Kamber and Webb, 2001). The Y/Ho ratios for the Shahejie carbonates are in the range of 28–45 (Table 2), and nearly all of the Shahejie Y/Ho ratios are greater than those of freshwater carbonates of the Green River Formation (Bolhar and Van Kranendonk, 2007), and are slightly less than the values of marine carbonates. Thus, the depositional environment of the Shahejie carbonates was characterized by significant influxes of seawater into a lacustrine environment.

4.2.3 Post-depositional processes

Previous studies have shown that Cenozoic volcanic rocks are widely distributed in the Shahejie, Dongying, and Guantao formations in the Qikou depression. Diabase and basalt were found in wells Zhuang-24, Kou-14, Kou-34, Kou-42 (the wells sampled in the present study), Kou-43, Zhang-16, and Gangshen-7 (Xue and Gao, 2011; Li et al., 2010; Sun et al., 2008, 2007; Wang and Zhang, 2001; Gao, 1986). The widespread volcanic activity in the Cenozoic, and potentially contemporaneous faulting, exposed the Shahejie carbonates to hydrothermal fluids. Ding et al. (2007) considered that the maturity levels of alkanes in carbonate inclusions are related to geothermal activity. Yu (2010) presented evidence for hydrothermal fluids in the Shahejie clastic rocks, based on petrological features, vitrinite reflectance data, pyrolysis temperatures, and clay mineral analyses.

Europium is believed to be the only REE that changes its valency in near-surface environments (Brookins, 1989): Eu^{3+} reduces to Eu^{2+} under extremely reducing conditions. Temperatures above 200 °C are normally required to stabilize Eu^{2+} (Bau, 1996), and the Eu^{3+}/Eu^{2+} ratio, a measure of redox potential, is considerably less at elevated temperatures (Sverjensky, 1984). The ratio is less sensitive to changes in pH and pressure than in temperature. Therefore, highly reducing hydrothermal fluids are enriched in Eu (Olivarez and Owen, 1991; Michard and Albarède, 1986). The REE patterns of various hydrothermal fluids are similar, showing LREE enrichment and positive Eu anomalies. Recent studies have shown that hydrothermal fluids at mid-oceanic ridges are characterized by significant enrichments in LREEs and Eu (James and Elderfield, 1996; Mills and Elderfield, 1995). The REE patterns of samples from Well Kou-42 are similar to those of Oligocene–Miocene hydrothermal carbonates of the Qinghai-Tibet Plateau (Yi et al., 2008) and Early Paleozoic hydrothermal dolomites of the Tarim Basin (Han et al., 2009) (Fig. 5). Some marine carbonates influenced by hydrothermal fluids not only exhibit characteristic HREE enrichment, but also show conspicuous positive Eu anomalies (Kamber and Webb, 2001) (Fig. 5), as in two of the samples from Well Wang-38 (Fig. 3b).

Because seawater $^{87}Sr/^{86}Sr$ ratios are regulated mainly by riverine inputs of Sr via hydrothermal and tectonic processes, seawater strontium isotope concentrations are a geochemical proxy for such processes (Shields, 2007; Veizer et al., 1999). Enhanced continental weathering, especially the weathering of silicate minerals after glaciation, acts to increase seawater $^{87}Sr/^{86}Sr$ ratios (Anderson et al., 2000; Blum et al., 1998). Initial $^{87}Sr/^{86}Sr$ ratios for Eocene–Oligocene seawater are in the range 0.707 7–0.708 3 (McArthur et al., 2001), while the average $^{87}Sr/^{86}Sr$ ratio for rivers is 0.711 9 (Palmer and Edmond, 1989). Basic rocks, which form by the melting of mantle, usually show low $^{87}Sr/^{86}Sr$ ratios (mean value, 0.704 4) (Zhang et al., 2000). In addition, the almost consistently low $^{87}Sr/^{86}Sr$ ratios (0.708 001–0.710 893) for the carbonates in Well Kou-42 (Table 2, Fig. 6) suggest that their deposition was accompanied by significant inputs from seawater. However, the lower Es_1 carbonates from Well Wang-38, which are more strongly influenced by seawater, show higher $^{87}Sr/^{86}Sr$ ratios (0.710 282–0.710 585) than those of Well Kou-42 (Fig. 6), indicating that the low $^{87}Sr/^{86}Sr$ ratios from Well Kou-42 are the result of magmatic hydrothermal activity.

The formation temperatures of carbonates are determined by the homogenization temperatures of fluid inclusions, which

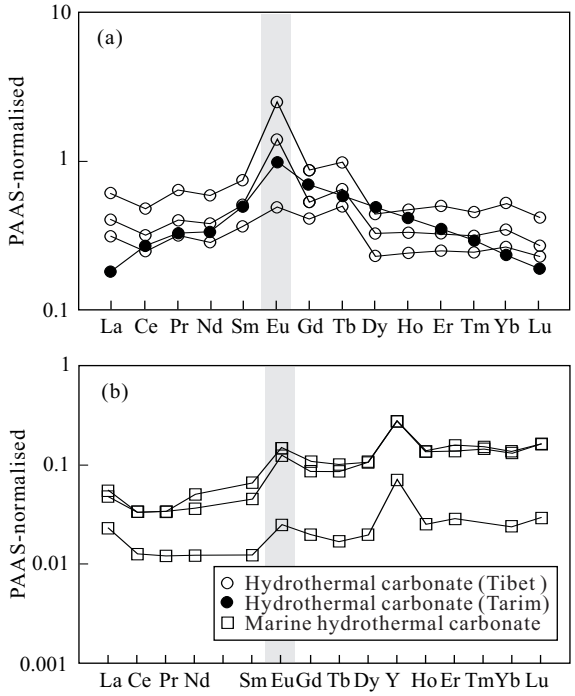

Figure 5. REE patterns of hydrothermal carbonates. Data sources: Han et al. (2009); Yi et al. (2008); Bolhar and Van Kranendonk (2007).

can then be compared with burial temperatures; in this way, we can generalize about the extent to which carbonates were influenced by hot fluids.

Paleogeotemperatures during deposition of Shahejie Paleogene sediments can be assessed using the following equation

$$H=(T_H-T_0)/G$$

where the burial depth H was 1 972.99–2 306.79 m (Table 1), the surface temperature T_0 was 15 °C (Gao et al., 2003), the average geothermal gradient G in the Qikou depression was 0.034 °C/m (Yang et al., 2014), and the burial paleogeotemperature T_H, which was determined using the above equation, was 82–93 °C. Most homogenization temperatures of fluid inclusions from rocks in Well Kou-42 are in the range of 120–150 °C, which is greater than the homogenization temperatures in Well Wang-38 (~100 °C) (Table 3, Fig. 7) and burial paleogeotemperatures (82–93 °C) in the Qikou depression. This indicates carbonates in Well Kon-42 have been influenced by diagenetic activity during diagenesis.

5 GLOBAL SEA-LEVEL FLUCTUATIONS

Although lake-level curves across the Eocene–Oligocene boundary in the Qikou depression are concordant with sea-level curves (Fig. 8), it has been suggested that a large-scale transgression occurred in eastern China during this time (Qiu et al., 1994). Global sea level rose rapidly during Es_3 times, then decreased across the Eocene–Oligocene boundary (Fig. 8). As a result, carbonates from Es_2 strata were largely unaffected by seawater, and show characteristics of freshwater sedimentary environments. During Es_1 time, a short period of transgression occurred (Fig. 8), which strongly influenced carbonate compositions: the REE patterns of two Es_1 samples from Well Wang-38 correspond

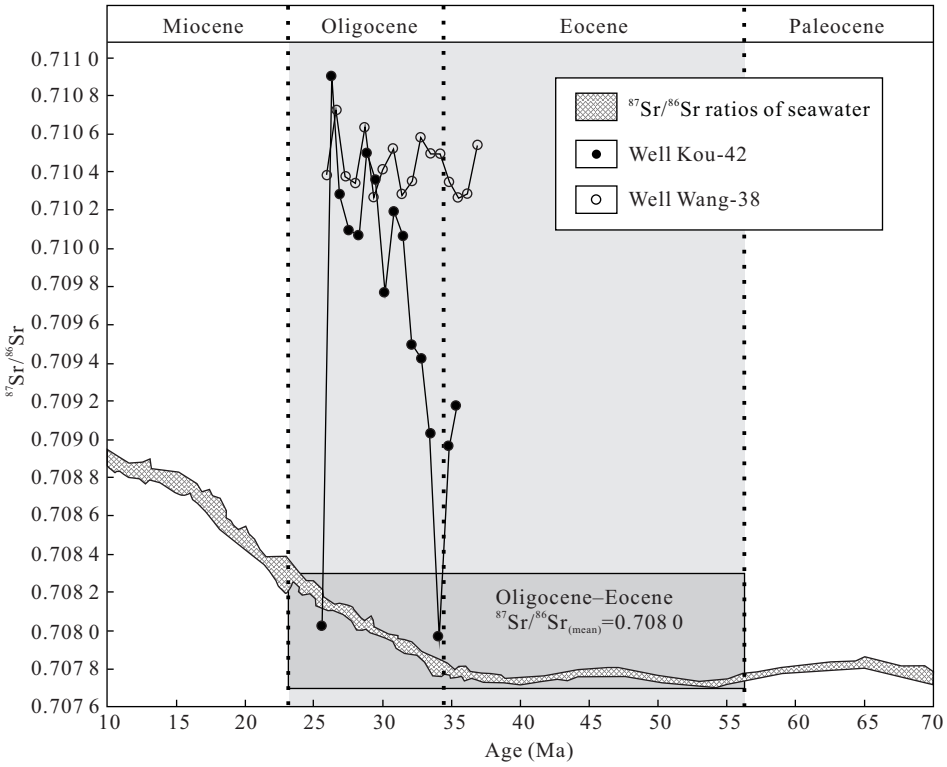

Figure 6. The $^{87}Sr/^{86}Sr$ ratios of seawater for the period 10–70 Ma (McArthur et al., 2001) and of the carbonates from the Shahejie Formation, Qikou depression.

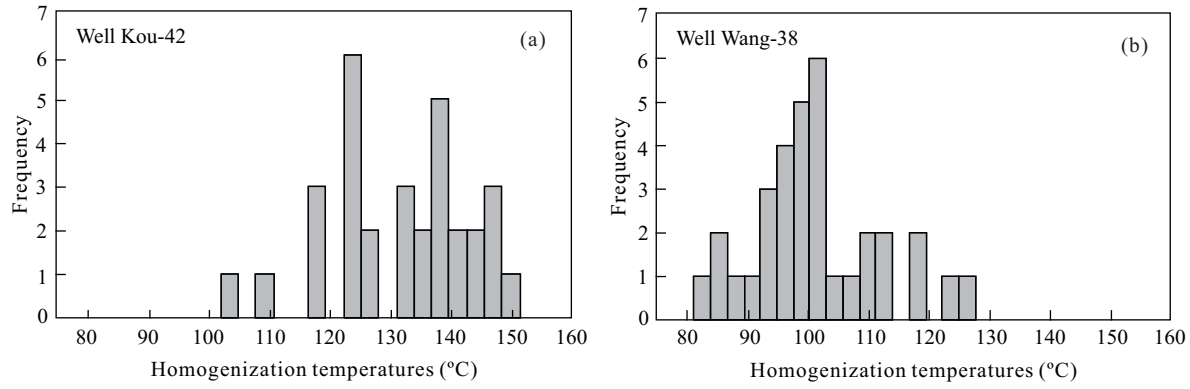

Figure 7. Histograms of homogenization temperatures of fluid inclusions in carbonates from the Shahejie Formation, Qikou depression.

exactly with those of marine carbonates (Fig. 3b).

Several studies have demonstrated that transgressions occurred worldwide in the Early Oligocene. During the EOT, two transgressive system tracts were deposited in the Jianghan Basin. In the basin, a deep-water lagoon formed in a deepening environment, as recorded by widely distributed halite interbedded with dark clasolite (Qiu et al., 1994). The Iwaki Formation, which is the lowermost part of the Eocene–Oligocene Shiramizu Group, Northeast Japan, consists of conglomeratic braided river sediments. This formation, along with two overlying formations in the group, exhibits a fining-upward succession that is interpreted as an overall transgressive sequence (Komatsubara, 2004). The Kachchh Basin, located along the western margin of India during Indo-Gondwana rifting, evolved as a peri-cratonic basin during the Mesozoic–Cenozoic. Oligocene deposits, approximately 100 m thick, consist of limestone/claystone/shale alternations representing a generally shallow marine environment (Biswas, 1982). The sea-level curves suggest that a short Early Oligocene

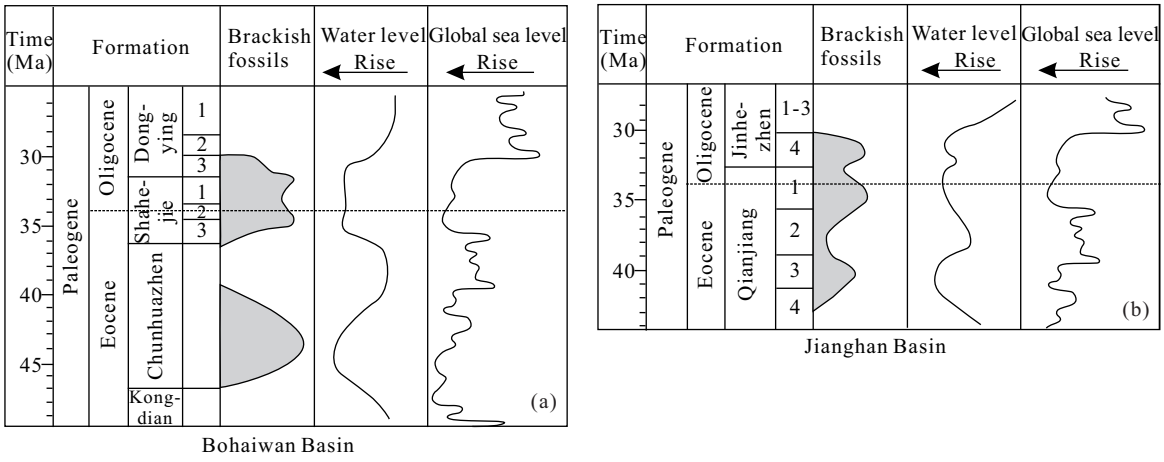

Figure 8. Occurrences of brackish-water fossils and curves for water level and global sea-level for the Bohaiwan Basin (upper panel) and the Jianghan Basin (lower panel) at the Eocene–Oligocene boundary, modified after Qiu et al. (1994).

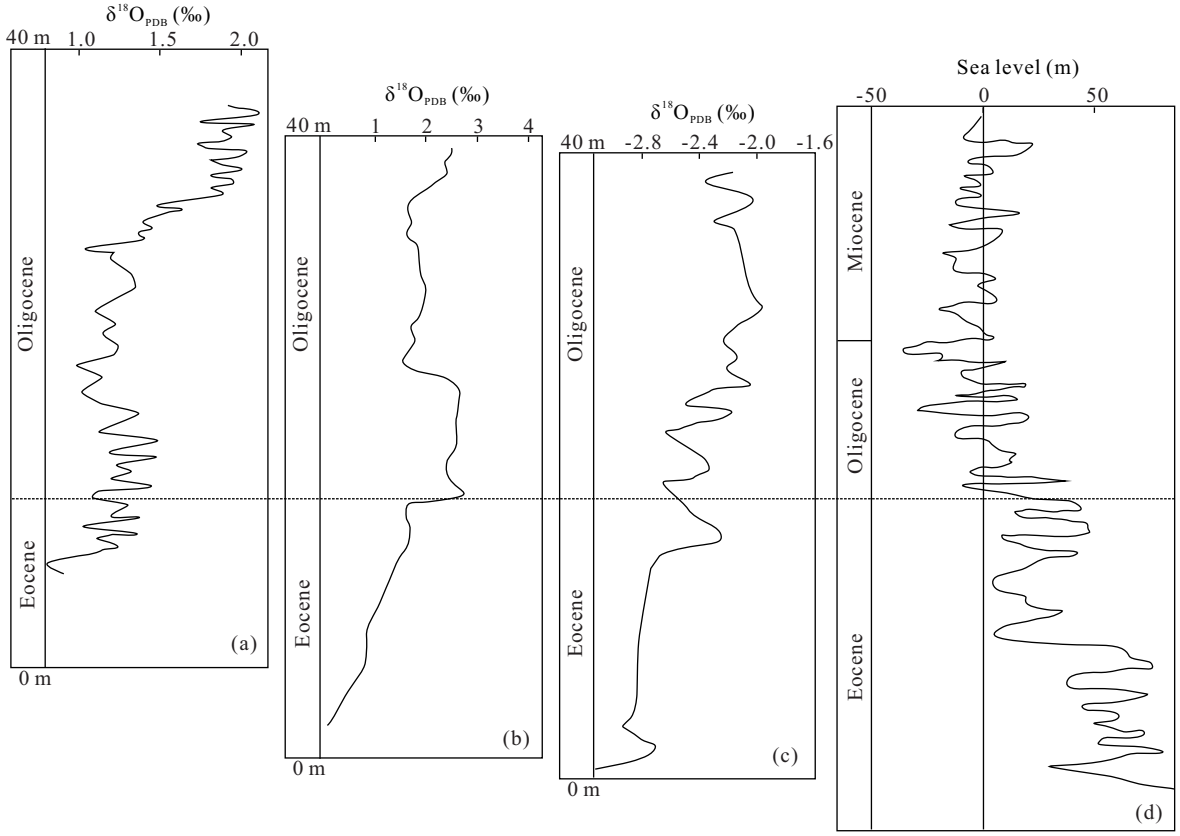

Figure 9. Oxygen isotope stratigraphy and sea-level fluctuations at the Eocene-Oligocene boundary. (a) Deep sea oxygen $\delta^{18}O$ record from ODP Site 1218 (after Coxall et al., 2005); (b) deep-sea benthic oxygen isotope curve (after Zachos et al., 1996); (c) the oxygen isotope record, biozonations and planktonic events identified in Tanzanian record (after Cotton and Pearson, 2011); (d) global sea level (blue) (after Miller et al., 2005).

transgression was followed by a major drop in sea level in Mid-Oligocene times (Pandey et al., 2010). The Early Oligocene transgression may have been caused by a brief temperature rise. Based on the work of Coxall et al. (2005), Zachos et al. (1996), and Miller et al. (2005), we have developed $\delta^{18}O$ curves (Fig. 9) for the Eocene–Oligocene boundary. Overall, the sea level fell during the EOT, but rose rapidly in the early Oligocene due to increased temperatures.

6 CONCLUSION

We measured the REE concentrations and $^{87}Sr/^{86}Sr$ ratios in carbonates of the Shahejie Formation to assess depositional conditions and post-depositional processes in the Qikou depression (Bohaiwan Basin, eastern China) at the Eocene-Oligocene boundary. La_{PAAS}/Yb_{PAAS} is variable, and most of the samples have similar REE patterns with LREE enrichment and HREE depletion. The relatively flat REE patterns with variable La and Ce anomalies indicate that the Shahejie carbonates were deposited in a lacustrine environment rather than a marine environment. The positive Y anomaly and Y/Ho ratios are higher than those of lacustrine carbonates and are similar to those of marine carbonates, suggesting that diagenetic fluids in the carbonates were influenced by seawater. Carbonates from Well Kou-42 show a positive Eu anomaly, low $^{87}Sr/^{86}Sr$ ratios, and high homogenization temperatures, implying that these carbonates were affected by hydrothermal fluids. During the Eocene–Oligocene transition, global sea level was generally falling; however, a brief period of worldwide temperature increase in the Early Oligocene caused a rapid sea-level rise.

ACKNOWLEDGMENTS

We thank the staff of the State Key Laboratory of Geological Processes and Mineral Resources, China University of Geosciences, Wuhan, China, for their advice and assistance during isotopic analysis. This work was financially supported by the National Natural Science Foundation of China (No. 41502145), and the Education Department of Jilin Province (Jijiaokehezi, No. 2016-313). The final publication is available at Springer via https://doi.org/10.1007/s12583-017-0759-z.

REFERENCES CITED

Alibo, D. S., Nozaki, Y., 2004. Dissolved Rare Earth Elements in the South China Sea: Geochemical Characterization of the Water Masses. *Deep Sea Research Part I*, 51: 559–576. https://doi.org/10.1016/j.dsr.2003.11.004

Anderson, S. P., Drever, J. I., Frost, C. D., et al., 2000. Chemical Weathering in the Foreland of a Retreating Glacier. *Geochimica et Cosmochimica Acta*, 64(7): 1173–1189. https://doi.org/10.1016/s0016-7037(99)00358-0

Bau, M., 1996. Controls on the Fractionation of Isovalent Trace Elements in Magmatic and Aqueous Systems: Evidence from Y/Ho, Zr/Hf, and Lanthanide Tetrad Effect. *Contributions to Mineralogy and Petrology*, 123(3): 323–333. https://doi.org/10.1007/s004100050159

Bau, M., Dulski, P., 1999. Comparing Yttrium and Rare Earths in Hydrothermal Fluids from the Mid-Atlantic Ridge: Implications for Y and REE Behaviour during Near-Vent Mixing and for the Y/Ho Ratio of Proterozoic Seawater. *Chemical Geology*, 155(1/2): 77–90. https://doi.org/10.1016/s0009-2541(98)00142-9

Bau, M., Möller, P., 1993. Rare Earth Element Systematics of the Chemically Precipitated Component in Early Precambrian Iron Formations and the Evolution of the Terrestrial Atmosphere-Hydrosphere-Lithosphere System. *Geochimica et Cosmochimica Acta*, 57(10): 2239–2249. https://doi.org/10.1016/0016-7037(93)90566-f

Bellanca, A., Masetti, D., Neri, R., 1997. Rare Earth Elements in Limestone/Marlstone Couplets from the Albian-Cenomanian Cismon Section (Venetian Region, Northern Italy): Assessing REE Sensitivity to Environmental Changes. *Chemical Geology*, 141(3/4): 141–152. https://doi.org/10.1016/s0009-2541(97)00058-2

Biswas, S. K., 1982. Rift Basins in Western Margin of India and their Hydrocarbon Prospects with Special Reference to Kutch Basin. *AAPG Bulletin*, 66(10): 1497–1513. https://doi.org/10.1306/03b5a976-16d1-11d7- 8645000102c1865d

Blum, J. D., Gazis, C. A., Jacobson, A. D., et al., 1998. Carbonate Versus Silicate Weathering in the Raikhot Watershed within the High Himalayan Crystalline Series. *Geology*, 26(5): 411–413. https://doi.org/10.1130/0091-7613(1998)026<0411:cvswit>2.3.co;2

Bolhar, R., Hofmann, A., Woodhead, J., et al., 2002. Pb- and Nd-Isotope Systematics of Stromatolitic Limestones from the 2.7 Ga Ngezi Group of the Belingwe Greenstone Belt: Constraints on Timing of Deposition and Provenance. *Precambrian Research*, 114(3/4): 277–294. https://doi.org/10.1016/s0301-9268(01)00229-7

Bolhar, R., Kamber, B. S., Moorbath, S., et al., 2004. Characterisation of Early Archaean Chemical Sediments by Trace Element Signatures. *Earth and Planetary Science Letters*, 222(1): 43–60. https://doi.org/10.1016/j.epsl.2004.02.016

Bolhar, R., Van Kranendonk, M. J., 2007. A Non-Marine Depositional Setting for the Northern Fortescue Group, Pilbara Craton, Inferred from Trace Element Geochemistry of Stromatolitic Carbonates. *Precambrian Research*, 155(3/4): 229–250. https://doi.org/10.1016/j.precamres.2007.02.002

Bonnot-Courtois, C., Flicoteaux, R., 1989. Distribution of Rare-Earth and Some Trace Elements in Tertiary Phosphorites from the Senegal Basin and Their Weathering Products. *Chemical Geology*, 75(4): 311–328. https://doi.org/10.1016/0009-2541(89)90004-1

Brenchley, P. J., Carden, G. A., Hints, L., et al., 2003. High-Resolution Stable Isotope Stratigraphy of Upper Ordovician Sequences: Constraints on the Timing of Bioevents and Environmental Changes Associated with Mass Extinction and Glaciation. *Geological Society of America Bulletin*, 115(1): 89–104. https://doi.org/10.1130/0016-7606(2003)115< 0089:hrsiso>2.0.co;2

Brookins, D. G., 1989. Aqueous Geochemistry of Rare Earth Elements. *Reviews in Mineralogy and Geochemistry*, 21(1): 201–225

Chen, S. Z., Gao, X. C., Qiu, D. Z., 1982. A Preliminary Study in China's Eogene Transitional Facies. *Oil & Gas Geology*, 3(4): 343–349 (in Chinese with English Abstract)

Cotton, L. J., Pearson, P. N., 2011. Extinction of Larger Benthic Foraminifera at the Eocene/Oligocene Boundary. *Palaeogeography, Palaeoclimatology, Palaeoecology*, 311(3/4): 281–296. https://doi.org/10.1016/j.palaeo.2011.09.008

Coxall, H. K., Wilson, P. A., Pälike, H., et al., 2005. Rapid Stepwise Onset of Antarctic Glaciation and Deeper Calcite Compensation in the Pacific Ocean. *Nature*, 433(7021): 53–57. https://doi.org/10.1038/nature03135

Curtis, C. D., Coleman, M. L., Love, L. G., 1986. Pore Water Evolution during Sediment Burial from Isotopic and Mineral Chemistry of Calcite, Dolomite and Siderite Concretions. *Geochimica et Cosmochimica Acta*, 50(10): 2321–2334. https://doi.org/10.1016/0016-7037(86)90085-2

Ding, W. W., Dai, J. X., Chu, F. Y., et al., 2007. Geochemical Characteristics of the Fluid Inclusions in the Gangxi Fault Belt Huanghua Depression, Bohai Bay Basin, China. *Acta Petrologica Sinica*, 23(9): 2287–2295 (in Chinese with English Abstract)

Drummond, C. N., Patterson, W. P., Walker, J. C. G., 1995. Climatic Forcing of Carbon-Oxygen Isotopic Covariance in Temperate-Region Marl Lakes. *Geology*, 23(11): 1031–1034. https://doi.org/10.1130/0091-7613(1995)023<1031:cfocoi>2.3.co;2

Elderfield, H., 1986. Strontium Isotope Stratigraphy. *Palaeogeography, Palaeoclimatology, Palaeoecology*, 57(1): 71–90 https://doi.org/10.1016/0031-0182(86)90007-6

Frimmel, H. E., 2009. Trace Element Distribution in Neoproterozoic Carbonates as Palaeoenvironmental Indicator. *Chemical Geology*, 258(3/4): 338–353. https://doi.org/10.1016/j.chemgeo.2008.10.033

Gao, Y. Q., Ou, G. X., Tan, S. Q., et al., 2003. Research on the Charge Times and Stages of Oil and Gas Reservoir in Lower Es_1 of Baishuitou Structure at West Slope in Qikou Depression. *Acta Petrologica Sinica*, 19(2): 359–365 (in Chinese with English Abstract)

Gao, Z. Y., 1986. The Tertiary Blind Volcanic Rocks in Huanghua Depression and Their Bearing on Tectonic Setting. *Acta Petrologica Sinica*, 2(4): 14–30 (in Chinese with English Abstract)

Ge, L., Jiang, S. Y., Swennen, R., et al., 2010. Chemical Environment of Cold Seep Carbonate Formation on the Northern Continental Slope of South China Sea: Evidence from Trace and Rare Earth Element Geochemistry. *Marine Geology*, 277(1/2/3/4): 21–30. https://doi.org/10.1016/j.margeo.2010.08.008

German, C. R., Elderfield, H., 1990. Application of the Ce Anomaly as a Paleoredox Indicator: The Ground Rules. *Paleoceanography*, 5(5): 823–833. https://doi.org/10.1029/pa005i005p00823

Grandjean, P., Cappetta, H., Michard, A., et al., 1987. The Assessment of REE Patterns and $^{143}Nd/^{144}Nd$ Ratios in Fish Remains. *Earth and Planetary Science Letters*, 84(2/3): 181–196. https://doi.org/10.1016/0012-821x(87)90084-7

Haley, B. A., Klinkhammer, G. P., McManus, J., 2004. Rare Earth Elements in Pore Waters of Marine Sediments. *Geochimica et Cosmochimica Acta*, 68(6): 1265–1279. https://doi.org/10.1016/j.gca.2003.09.012

Han, Y. X., Li, Z., Han, D. L., et al., 2009. REE Characteristics of Matrix Dolomites and Its Origin of Lower Ordovician in Eastern Tabei Area, Tarim Basin. *Acta Petrologica Sinica*, 25(10): 2405–2416 (in Chinese with English Abstract)

Hofmann, A., Bolhar, R., 2007. Carbonaceous Cherts in the Barberton Greenstone Belt and Their Significance for the Study of Early Life in the Archean Record. *Astrobiology*, 7(2): 355–388. https://doi.org/10.1089/ast.2005.0288

James, R. H., Elderfield, H., 1996. Chemistry of Ore-Forming Fluids and Mineral Formation Rates in an Active Hydrothermal Sulfide Deposit on the Mid-Atlantic Ridge. *Geology*, 24(12): 1147–1150. https://doi.org/10.1130/0091-7613(1996)024<1147:cooffa>2.3.co;2

Kamber, B. S., Bolhar, R., Webb, G. E., 2004. Geochemistry of Late Archean Stromatolites from Zimbabwe: Evidence for Microbial Life in Restricted Epicontinental Seas. *Precambrian Research*, 132(4): 379–399. https://doi.org/10.1016/j.precamres.2004.03.006

Kamber, B. S., Webb, G. E., 2001. The Geochemistry of Late Archaean Microbial Carbonate: Implications for Ocean Chemistry and Continental Erosion History. *Geochimica et Cosmochimica Acta*, 65(15): 2509–2525. https://doi.org/10.1016/s0016-7037(01)00613-5

Komatsubara, J., 2004. Fluvial Architecture and Sequence Stratigraphy of the Eocene to Oligocene Iwaki Formation, Northeast Japan: Channel-Fills Related to the Sea-Level Change. *Sedimentary Geology*, 168: 109–123. https://doi.org/10.1016/j.sedgeo.2004.03.005

Lawrence, M. G., Greig, A., Collerson, K. D., et al., 2006. Rare Earth Element and Yttrium Variability in South East Queensland Waterways. *Aquatic Geochemistry*, 12(1): 39–72. https://doi.org/10.1007/s10498-005-4471-8

Li, D. L., Tan, X. F., Xia, M. Q., et al., 2010. Sedimentary Characteristics and Genesis of Lacustrine Dolomite in the Fourth Member of Shahejie Formation in Dongying Sag. *Fault-Block Oil & Gas Field*, 17(4): 418–422 (in Chinese with English Abstract)

Li, C. F., Xiao, J. F., 1988. Study on Shahejie Formation's Paleosalinity in Dongying Basin of Shengli Oilfield by Trace Element. *Acta Sedimentologica Sinica*, 6(4): 100–106 (in Chinese with English Abstract)

Li, G. J., Chen, J., Ji, J. F., et al., 2007. Global Cooling Forced Increase in Marine Strontium Isotopic Ratios: Importance of Mica Weathering and a Kinetic Approach. *Earth and Planetary Science Letters*, 254(3/4): 303–312. https://doi.org/10.1016/j.epsl.2006.11.045

Li, M., Lou, Z. H., Zhu, R., et al., 2014. Distribution and Geochemical Characteristics of Fluids in Ordovician Marine Carbonate Reservoirs of the Tahe Oilfield. *Journal of Earth Science*, 25(3): 486–494. https://doi.org/10.1007/s12583-014-0453-3

Li, S. G., Wu, T., Fang, W. J., et al., 1991. Petroleum Geology of China (Vol. 4) Dagang Oil Field. Petroleum Industry Press, Beijing. 1–109 (in Chinese)

Li, Y. X., Lu, Z. S., Wang, D., et al., 1997. Study on Terrestrial Trace Fossils and Sedimentary Environment in Liaohe Basin. Petroleum Industry Press, Beijing. 1–23 (in Chinese)

MacLeod, K. G., Huber, B. T., 1996. Strontium Isotopic Evidence for Extensive Reworking in Sediments Spanning the Cretaceous-Tertiary Boundary at ODP Site 738. *Geology*, 24(5): 463–466. https://doi.org/10.1130/0091-7613(1996)024<0463:siefer>2.3.co;2

McArthur, J. M., 1994. Recent Trends in Strontium Isotope Stratigraphy. *Terra Nova*, 6(4): 331–358. https://doi.org/10.1111/j.1365-3121.1994.tb00507.x

McArthur, J. M., Howarth, R. J., Bailey, T. R., 2001. Strontium Isotope Stratigraphy: LOWESS Version 3: Best Fit to the Marine Sr-Isotope Curve for 0–509 Ma and Accompanying Look-up Table for Deriving Numerical Age. *The Journal of Geology*, 109(2): 155–170. https://doi.org/10.1086/319243

McArthur, J. M., Walsh, J. N., 1984. Rare-Earth Geochemistry of Phosphorites. *Chemical Geology*, 47(3/4): 191–220. https://doi.org/10.1016/0009-2541(84)90126-8

McLennan, S. M., 1989. Rare Earth Elements in Sedimentary Rocks: Influence of Provenance and Sedimentary Processes. *Reviews in Mineralogy and Geochemistry*, 21(1): 169–200

Michard, A., Albarède, F., 1986. The REE Content of Some Hydrothermal Fluids. *Chemical Geology*, 55(1/2): 51–60. https://doi.org/10.1016/0009-2541(86)90127-0

Miller, K. G., Kominz, M. A., Browning, J. V., et al., 2005. The Phanerozoic Record of Global Sea-Level Change. *Science*, 310(5752): 1293–1298. https://doi.org/10.1126/science.1116412

Mills, R. A., Elderfield, H., 1995. Rare Earth Element Geochemistry of Hydrothermal Deposits from the Active TAG Mound, 26°N Mid-Atlantic Ridge. *Geochimica et Cosmochimica Acta*, 59(17): 3511–3524. https://doi.org/10.1016/0016-7037(95)00224-n

Nozaki, Y., Lerche, D., Alibo, D. S., et al., 2000. The Estuarine Geochemistry of Rare Earth Elements and Indium in the Chao Phraya River, Thailand. *Geochimica et Cosmochimica Acta*, 64(23): 3983–3994. https://doi.org/10.1016/s0016-7037(00)00473-7

Nozaki, Y., Zhang, J., Amakawa, H., 1997. The Fractionation between Y and Ho in the Marine Environment. *Earth and Planetary Science Letters*, 148(1/2): 329–340. https://doi.org/10.1016/s0012-821x(97)00034-4

Olivarez, A. M., Owen, R. M., 1991. The Europium Anomaly of Seawater:

Implications for Fluvial Versus Hydrothermal REE Inputs to the Oceans. *Chemical Geology*, 92(4): 317–328. https://doi.org/10.1016/0009-2541(91)90076-4

Palmer, M. R., Edmond, J. M., 1989. The Strontium Isotope Budget of the Modern Ocean. *Earth and Planetary Science Letters*, 92(1): 11–26. https://doi.org/10.1016/0012-821x(89)90017-4

Palmer, M. R., Elderfield, H., 1986. Rare Earth Elements and Neodymium Isotopes in Ferromanganese Oxide Coatings of Cenozoic Foraminifera from the Atlantic Ocean. *Geochimica et Cosmochimica Acta*, 50(3): 409–417. https://doi.org/10.1016/0016-7037(86)90194-8

Pandey, D. K., Rajan, S., Pandey, A., 2010. Seismic Imaging of Paleogene Sediments of Kachchh Shelf (Western Indian Margin) and Their Correlation with Sea-Level Fluctuations. *Marine and Petroleum Geology*, 27(6): 1166–1174. https://doi.org/10.1016/j.marpetgeo.2010.02.002

Piepgras, D. J., Jacobsen, S. B., 1992. The Behavior of Rare Earth Elements in Seawater: Precise Determination of Variations in the North Pacific Water Column. *Geochimica et Cosmochimica Acta*, 56(5): 1851–1862. https://doi.org/10.1016/0016-7037(92)90315-a

Pu, X. G., Zhou, L. H., Xiao, D. Q., et al., 2011. Lacustrine Carbonates in the Southwest Margin of Qikou Sag, Huanghua Depression, Bohai Bay Basin. *Petroleum Exploration and Development*, 38(2): 136–144 (in Chinese with English Abstract)

Qiu, S. Y., Lu, B. L., Chen, Y. C., 1994. The Transgression from Upper Cretaceous to Paleogene in the East of China. *Marine Geology & Quaternary Geology*, 14(1): 97–106 (in Chinese)

Ren, L. Y., Lin, G. F., Zhao, Z. Q., et al., 2000. Early Tertiary Marine Transgression in Dongpu Depression. *Acta Palaeontologica Sinica*, 39(4): 553–557 (in Chinese with English Abstract)

Schmitz, B., Åberg, G., Werdelin, L., et al., 1991. $^{87}Sr/^{86}Sr$, Na, F, Sr, and La in Skeletal Fish Debris as a Measure of the Paleosalinity of Fossil-Fish Habitats. *Geological Society of America Bulletin*, 103(6): 786–794. https://doi.org/10.1130/0016-7606(1991)103<0786:ssnfsa>2.3.co;2

Shaw, H. F., Wasserburg, G. J., 1985. Sm-Nd in Marine Carbonates and Phosphates: Implications for Nd Isotopes in Seawater and Crustal Ages. *Geochimica et Cosmochimica Acta*, 49(2): 503–518. https://doi.org/10.1016/0016-7037(85)90042-0

Shields, G. A., 2007. A Normalised Seawater Strontium Isotope Curve: Possible Implications for Neoproterozoic-Cambrian Weathering Rates and the Further Oxygenation of the Earth. *eEarth*, 2(2): 35–42. https://doi.org/10.5194/ee-2-35-2007

Shields, G. A., Webb, G. E., 2004. Has the REE Composition of Seawater Changed over Geological Time?. *Chemical Geology*, 204(1/2): 103–107. https://doi.org/10.1016/j.chemgeo.2003.09.010

Shields, G., Stille, P., 2001. Diagenetic Constraints on the Use of Cerium Anomalies as Palaeoseawater Redox Proxies: An Isotopic and REE Study of Cambrian Phosphorites. *Chemical Geology*, 175(1/2): 29–48. https://doi.org/10.1016/s0009-2541(00)00362-4

Sholkovitz, E., Shen, G. T., 1995. The Incorporation of Rare Earth Elements in Modern Coral. *Geochimica et Cosmochimica Acta*, 59(13): 2749–2756. https://doi.org/10.1016/0016-7037(95)00170-5

Stille, P., 1992. Nd-Sr Isotope Evidence for Dramatic Changes of Paleocurrents in the Atlantic Ocean during the Past 80 M.y.. *Geology*, 20(5): 387–390. https://doi.org/10.1130/0091-7613(1992)020<0387:nsiefd>2.3.co;2

Stille, P., Riggs, S. R., Clauer, N., et al., 1994. Sr and Nd Isotopic Analysis of Phosphorite Sedimentation through one Miocene High-Frequency Depositional Cycle on the North Carolina Continental Shelf. *Marine Geology*, 117(1/2/3/4): 253–273. https://doi.org/10.1016/0025-3227(94)90019-1

Stille, P., Steinmann, M., Riggs, S. R., 1996. Nd Isotope Evidence for the Evolution of the Paleocurrents in the Atlantic and Tethys Oceans during the Past 180 Ma. *Earth and Planetary Science Letters*, 144(1/2): 9–19. https://doi.org/10.1016/0012-821x(96)00157-4

Sun, Y., Zhong, J. H., Yuan, X. C., et al., 2008. Analysis on Sequence Stratigraphy of Lacustrine Carbonate in the First Member of Shahejie Formation in Huimin Sag. *Acta Petrolei Sinica*, 29(2): 213–218 (in Chinese with English Abstract)

Sun, Y., Zhong, J. H., Yuan, X. C., 2007. Genesis of the Dolostones from the First Member of the Shahejie Formation in the Huimin Depression, Shandong. *Sedimentary Geology and Tethyan Geology*, 27(3): 78–84 (in Chinese with English Abstract)

Sun, Z. C., Yang, F., Zhang, Z. H., et al., 1997. Depositional Environment and Generation of Oil and Gas of Cenozoic Salinized Lakes. Petroleum Industry Press, Beijing. 1–338 (in Chinese)

Sverjensky, D. A., 1984. Europium Redox Equilibria in Aqueous Solution. *Earth and Planetary Science Letters*, 67(1): 70–78. https://doi.org/10.1016/0012-821x(84)90039-6

Taylor, S. R., McLennan, S. M., 1985. The Continental Crust: Its Composition and Evolution. Blackwell, Cambridge. 1–321

Tong, X. G., 1985. Doubts about the Validity of Paleogene Transgression in the Eastern China. *Geological Review*, 31(3): 261–267 (in Chinese with English Abstract)

Van Kranendonk, M. J., Webb, G. E., Kamber, B. S., 2003. Geological and Trace Element Evidence for a Marine Sedimentary Environment of Deposition and Biogenicity of 3.45 Ga Stromatolitic Carbonates in the Pilbara Craton, and Support for a Reducing Archaean Ocean. *Geobiology*, 1(2): 91–108. https://doi.org/10.1046/j.1472-4669.2003.00014.x

Veizer, J., Ala, D., Azmy, K., et al., 1999. $^{87}Sr/^{86}Sr$, $\Delta^{13}C$ and $\Delta^{18}O$ Evolution of Phanerozoic Seawater. *Chemical Geology*, 161(1/2/3): 59–88. https://doi.org/10.1016/s0009-2541(99)00081-9

Veizer, J., Hoefs, J., Lowe, D. R., et al., 1989. Geochemistry of Precambrian Carbonates: II. Archean Greenstone Belts and Archean Sea Water. *Geochimica et Cosmochimica Acta*, 53(4): 859–871. https://doi.org/10.1016/0016-7037(89)90031-8

Wang, D. R., Zhang, Y. H., 2001. A Study on the Carbonate Cements within Reservoir in the External Metamorphic Belt of the Bohai Bay Oil/Gas-Bearing Region and Its Implications. *Petroleum Exploration and Development*, 28(2): 40–42 (in Chinese with English Abstract)

Webb, G. E., Kamber, B. S., 2000. Rare Earth Elements in Holocene Reefal Microbialites: A New Shallow Seawater Proxy. *Geochimica et Cosmochimica Acta*, 64(9): 1557–1565. https://doi.org/10.1016/s0016-7037(99)00400-7

Wright, J., Schrader, H., Holser, W. T., 1987. Paleoredox Variations in Ancient Oceans Recorded by Rare Earth Elements in Fossil Apatite. *Geochimica et Cosmochimica Acta*, 51(3): 631–644. https://doi.org/10.1016/0016-7037(87)90075-5

Wu, X. T., Ren, L. Y., 2004. The Tertiary Sea Way and New Reservoir Probe in Dongpu Depression as well as Its Surrounding Basins. *Acta Palaeontologica Sinica*, 43(1): 147–154 (in Chinese with English Abstract)

Xue, G. G., Gao, J. Z., 2011. Volcanism and Halite Genesis in Shahejie Formation of Paleaogene in Dongpu Depression. *Journal of Oil and Gas Technology*, 33(1): 53–75 (in Chinese with English Abstract)

Yang, Y., Gao, F. H., Pu, X. G., et al., 2013. Changes to Depositional Palaeoenvironments within the Qikou Depression (Bohaiwan Basin, China): Carbon and Oxygen Isotopes in Lacustrine Carbonates of the Palaeogene Shahejie Formation. *International Geology Review*, 55(15): 1909–1921. https://doi.org/10.1080/00206814.2013.805926

Yang, Y., Gao, F. H., Pu, X. G., et al., 2014. REE Characteristics and Genesis of

Dolostones from Paleogene Shahejie Formation in Qikou Depression. *Journal of China University of Petroleum* (*Edition of Natural Sciences*), 38(2): 1–9 (in Chinese with English Abstract).

Yao, Y. M., Xu, J. L., Shan, H. G., et al., 1992. A Discussion of the Paleogene Transgression in the Jiyang Depression, Shandong Province. *Acta Petrolei Sinica*, 13(2): 29–34 (in Chinese with English Abstract)

Yi, H. S., Lin, J. H., Zhao, X. X., et al., 2008. Geochemistry of Rare Earth Elements and Origin of Positive Europium Anomaly in Miocene-Oligocene Lacustrine Carbonates from Tuotuohe Basin of Tibetan Plateau. *Acta Sedimentologica Sinica*, 26(1): 1–10 (in Chinese with English Abstract)

Yu, Z. C., 2010. The Paleogene Thermal Fluid Activities and Their Impact on Clastic Reservoir in Qikou Sag: [Dissertation]. Jilin University, Changchun. 1–121 (in Chinese with English Abstract)

Yu, Z., 1982. Discovery of Calcareous Nanofossils in Liaohe Area. *Petroleum Exploration and Development*, 3: 82 (in Chinese)

Zachos, J. C., Quinn, T. M., Salamy, K. A., 1996. High-Resolution (104 Years) Deep-Sea Foraminiferal Stable Isotope Records of the Eocene-Oligocene Climate Transition. *Paleoceanography*, 11(3): 251–266. https://doi.org/10.1029/96pa00571

Zhang, G. D., Wang, H. Z., 1987. Transgression and sedimentary environment of Paleogene in Eastern China. Geological Publishing House, Beijing. 1–41 (in Chinese)

Zhang, J., Nozaki, Y., 1996. Rare Earth Elements and Yttrium in Seawater: ICP-MS Determinations in the East Caroline, Coral Sea, and South Fiji Basins of the Western South Pacific Ocean. *Geochimica et Cosmochimica Acta*, 60(23): 4631–4644. https://doi.org/10.1016/s0016-7037(96)00276-1

Zhang, Y. X., Li, X. D., Zhang, J., 2000. Basic Pluton and Its Tectonic Setting in Kaladala of West Tianshan Mountain, China. *Xinjiang Geology*, 18(3): 258–263 (in Chinese with English Abstract)

Zhao, C. L., Liu, M. H., 1988. Early Tertiary Microfacies of Sandbody and Diagenesis in Dongpu Depression. Petroleum University Publishing House, Dongying. 15 (in Chinese)

Zheng, R. C., Pan, Y. H., Zhao, C., et al., 2013. Carbon and Oxygen Isotope Stratigraphy of the Oxfordian Carbonate Rocks in Amu Darya Basin. *Journal of Earth Science*, 24(1): 42–56. https://doi.org/10.1007/s12583-013-0315-4